Comment on Li pellet conditioning in tokamak fusion test reactor

R. V. Budny
Princeton Plasma Physics Laboratory, Princeton, New Jersey 08543, USA

(Received 27 May 2011; accepted 9 July 2011; published online 9 September 2011)

Li pellet conditioning in TFTR results in a reduction of the edge electron density which allows increased neutral beam penetration, central heating, and fueling. Consequently, the temperature profiles became more peaked with higher central T_i, T_e, toroidal rotation, and neutron emission rates. © *2011 American Institute of Physics*. [doi:10.1063/1.3626541]

I. INTRODUCTION

Wall conditioning is helpful for achieving high plasma performance in tokamaks as measured by high temperatures, confinement times, and neutron emission. These beneficial effects result from reduced influx from the walls and lower impurity levels in the core plasma.

One of the wall conditioning techniques is the use of Li to coat the walls. There is a renewed interest in studying Li in various fusion test devices.[1] One technique for introducing Li is via pellet injection. This was pioneered in ALCATOR-CMOD where it was first used for impurity transport studies. Li pellet wall conditioning was tried in ALCATOR-CMOD Ohmic H-modes without a big effect except for reduction in H-mode threshold.[2] Li pellet wall conditioning was also tried in ALCATOR-CMOD with ICRF heated shots with peaked density profiles.[3] Enhanced energy confinement and fusion reactivity were seen.

Various conditioning techniques were used in TFTR. The technique which injected the highest amount of Li was injecting an aerosol from laser ablation of Li (DOLLOP).[4] Li pellet injection was also used extensively in TFTR. Strong improvements in performance were seen.[5] Typically small $\simeq$ 3mg pellets were injected before or after the high power phase of the plasma discharge. This paper discusses analysis of a series of TFTR shots using this technique.

II. SHOTS STUDIED

The shots studied here were a series of five well diagnosed TFTR shots. They showed rapid changes from poorly conditioned to well conditioned supershots. The shots had a flat top current of 2.5 MA and toroidal field of 5.1 T. Deuterium was the bulk hydrogenic species. Traces of hydrogen and tritium from recycling were also present. The shots were heated by neutral beam injection (NBI) of D^0 from 3.5 to 4.3 s. The first four had 19.0 MW injected with 56% of the power in the co-plasma direction and the fifth had 24.8 MW with 66% of the power injected in the co-plasma current direction.

Li pellets were fired into the shots after, and in all, but the first shot before the beam heating phase. Three of the shots had two pellets injected early. The timing can be seen from the traces of the measured central electron densities, as echoed in TRANSP, shown in Fig. 1.

III. ANALYSIS AND RESULTS

TRANSP analysis[6] was redone to incorporate several improvements recently added to the code. These include the ADAS atomic cross section data[7,8] which is more up-to-date than the Oak Ridge "Red Book" data used in TRANSP during the TFTR experimental campaign. Also the TEQ equilibrium solver[9] now in TRANSP gives more accurate numerical solutions to the Grad-Shafranov equations compared to the VMEC solver. Neither of these improvements had significant changes in the TRANSP results. The accuracy of the TRANSP analysis is indicated by the accuracy simulating the neutron emission rate. A comparison for the first shot of the series is shown in Fig. 2.

The source rate of D^+ within the last closed flux surface (LCFS) due to wall recycling is needed for the analysis. This is calculated from the measured D_α rate using the DEGAS code,[10] as shown in Fig. 3. The decrease in the peak rate from shot to shot in the series is correlated with the increase in the central electron density n_e during the NBI phase, shown in Fig. 1.

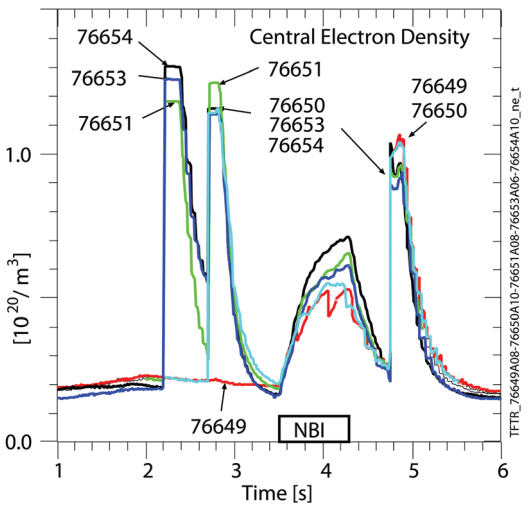

FIG. 1. (Color) Central electron densities. The truncation of the density near the pellets is due to the use of a time window around the injection times, which halts the TRANSP analysis. One Li pellet was injected into the post-NBI phase of all the shots. One Li pellet was injected into the pre-NBI phase of the second shot. Two Li pellets were injected into the pre-NBI phase of last three shots. Sawteeth effects are seen in the first shot of the series.

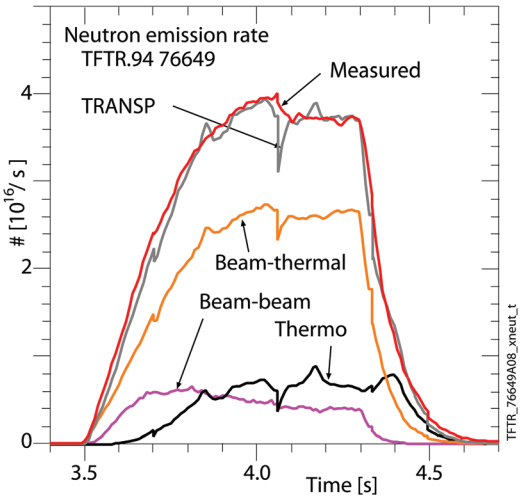

FIG. 2. (Color) Measured and computed neutron emission rates for the first (unconditioned) shot of the start of the conditioning series. The beam-thermal, beam-beam, and thermonuclear contributions to the TRANSP total are indicated. The approximate agreement between the measured and TRANSP simulated total neutron rate indicates accuracy of the TRANSP analysis. A sawtooth crash at 4.33 s causes dips in the neutron emission rates computed by TRANSP.

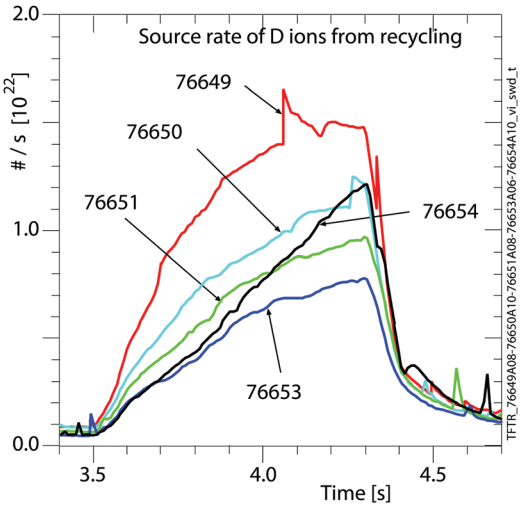

FIG. 3. (Color) Rate of D^4 ionizations within the LCFS from wall recycling calculated from measured D_α emission scaled by a constant to convert photons to ionizations within the LCFS. The constant is calculated by DEGAS modeling of D_α emission along five chords in similar plasmas.[10] The rate decreases more than a factor of two with conditioning.

The numbers of Li ions injected into the LCFS is calculated in TRANSP using the discontinuities of the measured electron density profiles n_e before and after each pellet. Example of the measured n_e and computed Li density n_{Li} profiles near the time of one of the pellet injections are shown in Fig. 4. The number of Li ions injected into the LCFS is calculated to be 4×10^{20}. The numbers of Li ions calculated this way for each of the pellets are given in Table I. The number of Li ions is calculated to decrease below 6×10^{17} by 3.7 s, i.e., 300 ms after the start of NBI. For comparison, the maximum number of thermal deuterons within the LCFS (during the NBI phase) is 4.0-5.4 $\times 10^{20}$ and the maximum number of fast beam ions is 1.8-2.3 $\times 10^{20}$.

The number of Li ions from each pellet is 5×10^{20}, so the TRANSP calculations indicate that most of the injected Li penetrates the LCFS. One source of uncertainty in the TRANSP calculation is the lack of measured Z_{eff} profiles during the Ohmic phases when the pellets are injected. The Z_{eff} profile during the NBI phase used in TRANSP is from the measured carbon density shape normalized by a calibrated chordal visible bremsstrahlung emission measurement.

Density profiles at the end of the NBI are shown in Fig. 5. A slight, but significant decrease in n_e outside of x (defined by the square-root of the toroidal flux) = 0.4 is seen in Fig. 5(a). The measured carbon impurity density n_C increases in the core (Fig. 5(b)), but the thermal deuterium density n_D also increases in the core (Fig. 5(c)). This is important for increasing the neutron emission rate.

The deposition rates of the beam neutrals depend sensitively on the n_e profile. Profiles of the deposition rates are shown in Fig. 6. The deposition rate in the core increases with conditioning. The electron source rate from ionizations caused by beam injection is shown in Fig. 7(a). The volume-average source rate of electrons in the core ($x < 0.2$) is about (1.3-1.4) $\times 10^{20}/\text{m}^3/\text{s}$ for the four shots (with $P_{NBI} = 19$ MW), and (1.7-2.0) $\times 10^{20}/\text{m}^3/\text{s}$ for the last shot (with $P_{NBI} = 24.8$ MW). These rates within 30% of the average rates of increase of n_e shown in Fig. 1 during the first 200 msec of beam injection. Thus beam ionization rates in the core can account for the rise in the central n_e during that time.

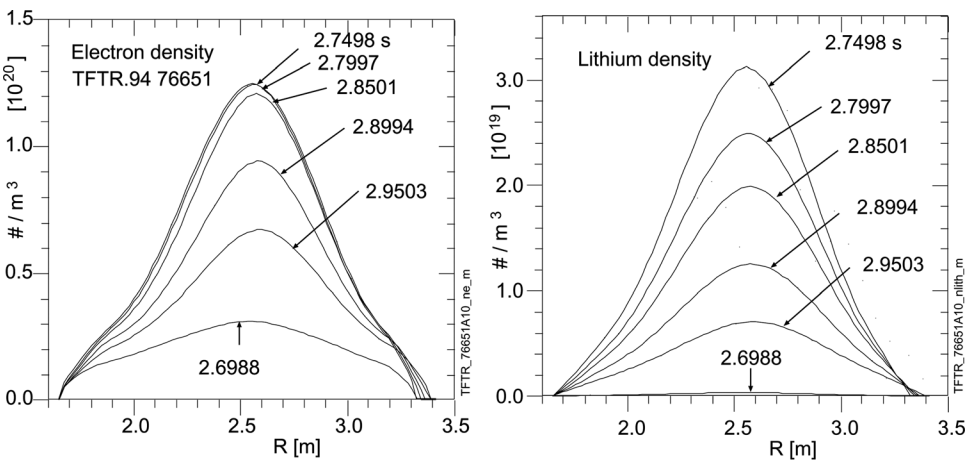

FIG. 4. Fits to the measured n_e and computed n_{Li} profiles for the second pre-NBI pellet in the third shot of the conditioning series.

TABLE I. Number of Li ions injected within the LCFS [10^{20}] and P_{NBI} [MW]. The number of Li ions is derived by TRANSP from the discontinuity in the measured n_e profiles before and after the injection. The Li is computed to exit the LCFS with a half-life of 200 ms.

Shot number Injection time [s]	1st pre-NBI 2.21	2nd pre-NBI 2.72	NBI 3.5-4.7	Post-NBI 4.76
76649	0	0	19.0	0.1
76650	0	4.5	19.0	3.7
76651	3.0	3.8	19.0	4.9
76653	3.4	1.3	19.0	3.7
76654	3.5	2.4	24.8	3.7

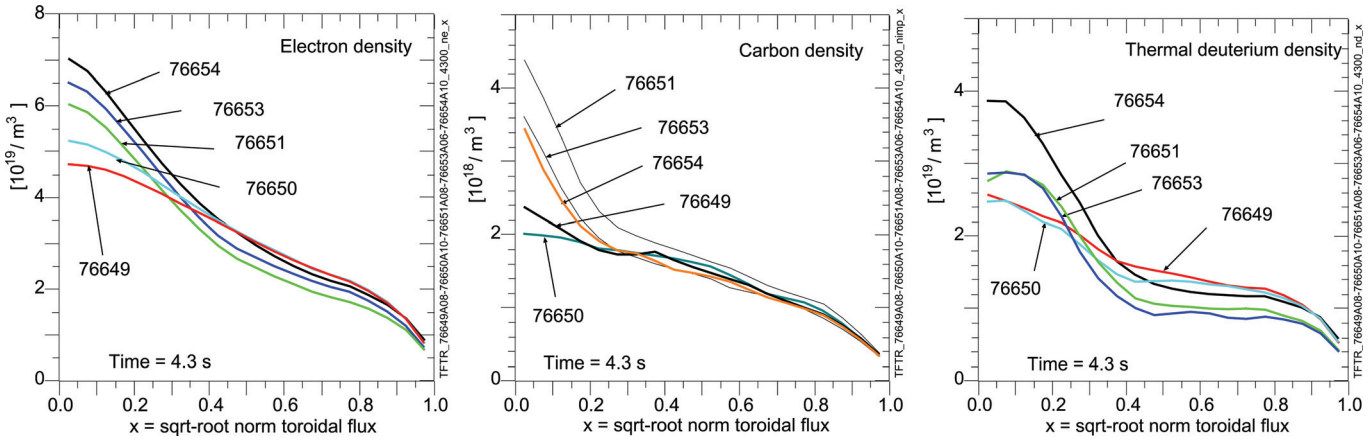

FIG. 5. (Color) Electron, carbon impurity, and thermal deuterium densities profiles at 4.3 s. The deuterium density is computed in TRANSP by local charge neutrality using the measured electron and carbon densities and computed beam ion densities.

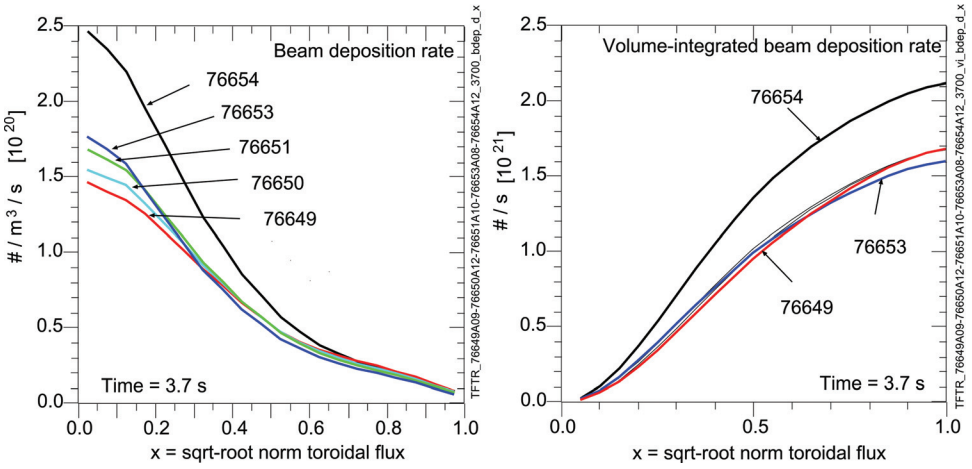

FIG. 6. (Color) Profiles of the beam deposition and volume-integrated deposition.

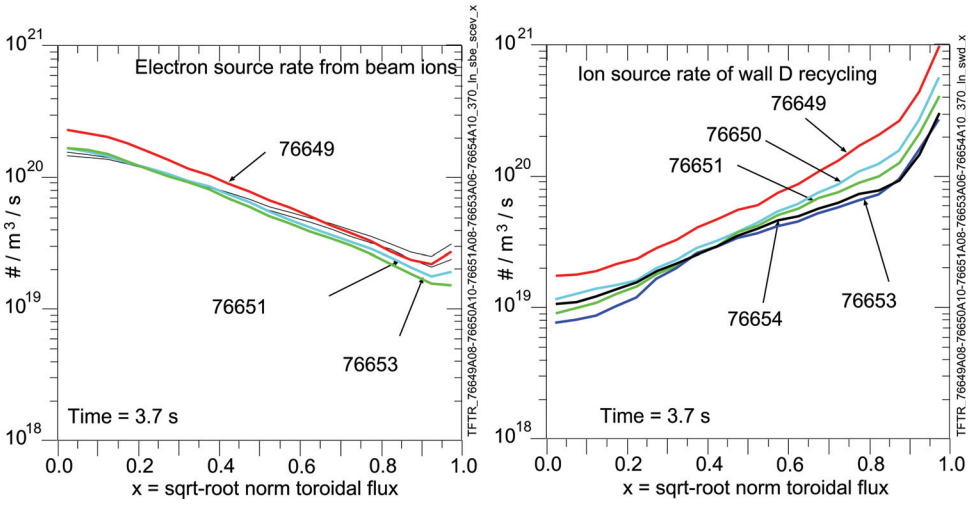

FIG. 7. (Color) Profiles at 3.7 s of electron ionizations of beam neutrals (direct + halo) and ionizations of deuterium from wall recycling (inferred from the measured D_α emission and DEGAS modeling). Recycling dominates outside x = 0.5 and beam fueling dominates inside.

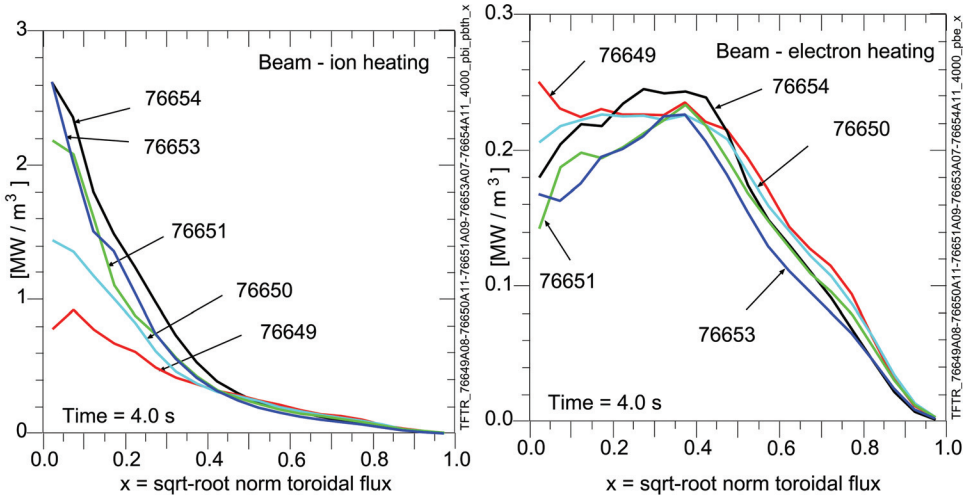

FIG. 8. (Color) Profiles at 4.0 s of beam heating of thermal ions and electrons.

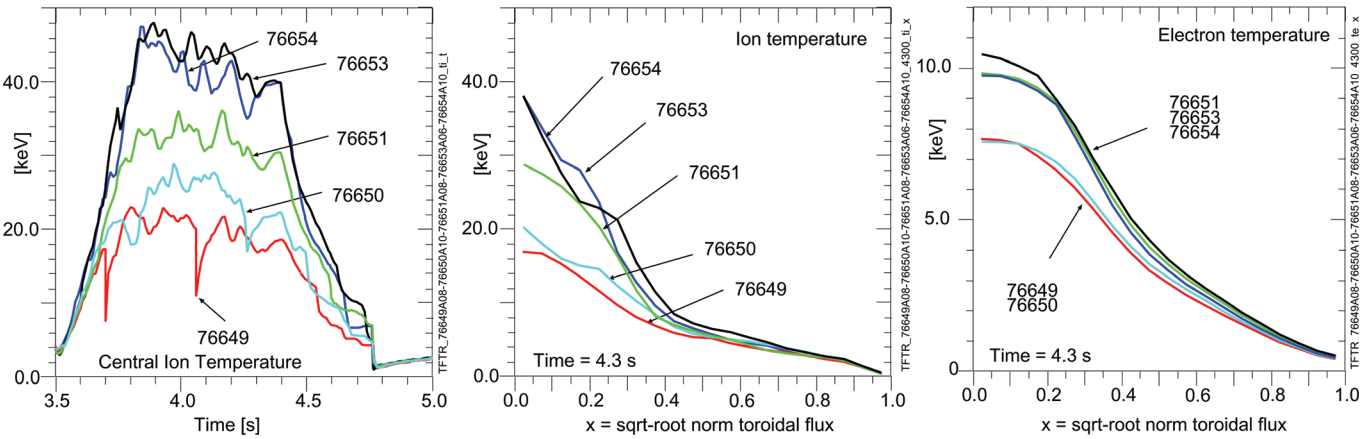

FIG. 9. (Color) Central ion temperatures in the core and ion and electron temperature profiles at 4.3 s.

For comparison, the estimated rate of ionizations from recycling deuterium is shown in Fig. 7(b).

Heating profiles from the NBI are shown in Fig. 8. The NBI heating of thermal ions in the core is considerably higher than that of (thermal) electrons. Higher rates of ion heating are achieved in the shots with better conditioning. The higher heating results in large central ion temperatures (Fig. 9). The peak values are doubled as a result of the Li pellet conditioning. The peak values for last two shots in the series are among the highest measured in TFTR. The electron temperature profiles measured from electron cyclotron emission (Fig. 9(c)) also become more peaked with higher central values. Since the beam-electron heating does not change significantly, the increase is due mainly to increased ion-electron energy transfer.

There is speculation[11] that with sufficient coverage of Li on the walls to prevent recycling, the temperature profiles will have reduced gradients in the core and high temperatures near the wall. A benefit of this could be reduced temperature gradient driven turbulence, high beta, and high fusion power. No tendency was observed with Li pellet conditioning in TFTR for either T_i or T_e to increase near the edge. This lack

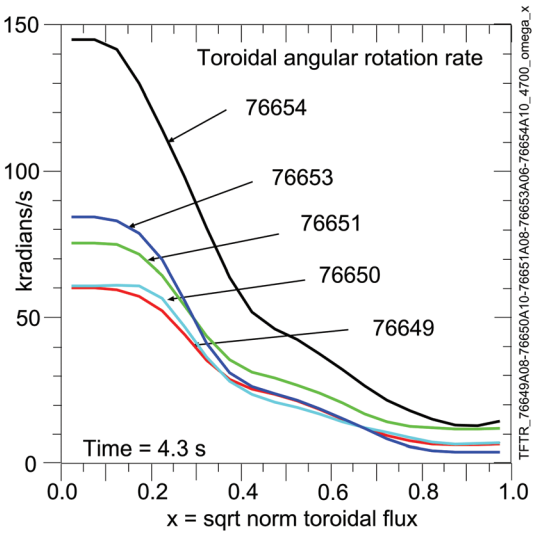

FIG. 10. (Color) Toroidal rotation rate profiles at 4.3 s.

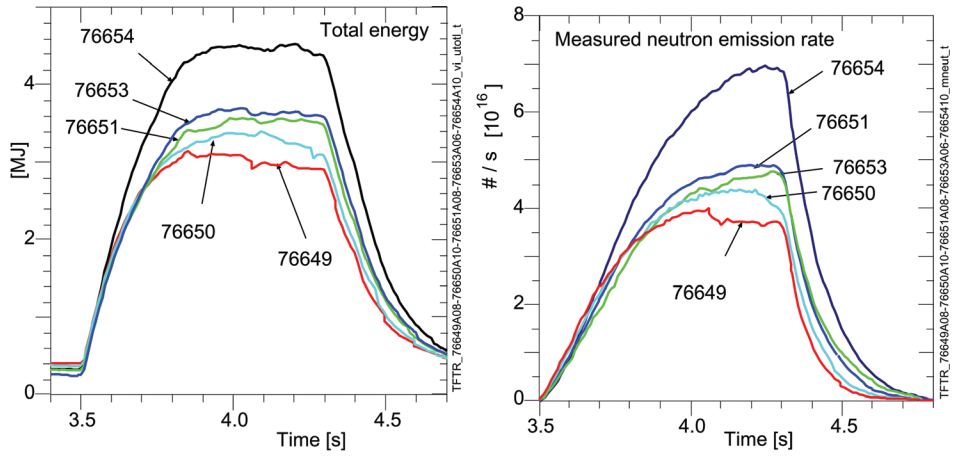

FIG. 11. (Color) Total stored energy and measured neutron emission rates.

of broadening of T_i or T_e could indicate that not enough Li ions were injected in this series to cause this effect.

The toroidal rotation profiles measured from the carbon impurity via charge-exchange spectroscopy increase with Li pellets. They are shown in Fig. 10.

The density of the moments of angular momentum decrease nearly a factor of two outside x = 0.4 and increase in the core with conditioning. The beam torque densities also decrease outside x = 0.4 and increase in the core with conditioning. Unlike the beam fueling rate, the beam torquing and heating rates increase gradually after the NBI starts. Thus the rates of increase of the central toroidal rotation and energies of the thermal plasma are not related simply to the torquing and heating rates. The higher central T_i results in higher total stored energy, and the higher central T_i and n_D result in higher neutron emission. These are shown in Fig. 11. The last shot in the series (76654) had higher P_{NBI} than the others, and the higher heating explains most of the increase above the earlier shots.

IV. SUMMARY

The TRANSP code is used to analyze data from a series of Li pellet conditioning in TFTR. The conditioning resulted in a reduction of the edge density. The TRANSP results show that this allowed increased neutral beam penetration, central heating, and fueling. This allows increased peaking of the density and temperature profiles, and higher central T_i, T_e, and neutron emission rates. The observation of more modest results of Li pellet conditioning in ALCATOR-CMOD can be attributed to the fact that NBI was not available.

ACKNOWLEDGMENTS

This paper is dedicated to Doug McCune, who died on July 16 when he and his bicycle collided with a car. This occurred near the end of a seven day, 500 mile biking "Ride for Runaways" organized as a charity drive for Anchor House, a local non-profit home for troubled youths. Doug had participated in this event during 15 previous summers. This summer he started an on-line fund raising capability for the charity. Besides being the brilliant mastermind of TRANSP and PTRANSP, he was a kind and considerate gentleman. This is a tragic loss for his family, friends, co-workers, and for magnetic fusion research.

This research is supported by the U.S. Department of Energy under contract number DE-AC02-09CH11466.

[1]The 2nd International Symposium on Lithium Applications for Fusion Devices" (Princeton, 2011), isla2011.pppl.gov/Worksh.
[2]J. A. Snipes, R. S. Granetz, M. Greenwald, I. H. Hutchinson, D. Garnier, J. A. Goetz, S. N. Golovato, A. Hubbard, J. H. Irby, B. LaBombard, T. Luke, E. S. Marmar, A. Niemczewski, P. C. Stek, Y. Takase, J. L. Terry, and S. M. Wolfe Nucl. Fusion **3**, 1039 (1994).
[3]Y. Takase, R. L. Boivin, P. T. Bombarda, P. T. Bonoli, C. Christensen, C. Fiore, D. Garnier, J. A. Goetz, S. N. Golovato, R. Granetz, M. Greenwald, S. F. Horne, A. Hubbard, I. H. Hutchinson, J. Irby, B. LaBombard, B. Lipschultz, E. Marmar, M. May, A. Mazurenko, G. McCracken, P. O' Shea, M. Porkolab, J. Reardon, J. Rice, C. Rost, J. Schachter, J. A. Snipes, P. Stek, J. Terry, R. Watterson, B. Welch, and S. Wolfe, Phys. Plasmas **4**, 1647 (1997).
[4]D. K. Mansfield, D. W. Johnson, B. Grek, H. W. Kugel, M. G. Bell, R. E. Bell, R. V. Budny, C. E. Bush, E. D. Fredrickson, K. W. Hill, D. L. Jassby, R. J. Maqueda, H. K. Park, A. T. Ramsey, E. J. Synakowski, G. Taylor, and G. A. Wurden, Nucl. Fusion **41**, 1823 (2001).
[5]J. A. Snipes, E. S. Marmar, M. G. Bell, R. V. Budny, K. W. Hill *et al.*, J. Nucl. Mater. **196–198**, 686 (1991).
[6]R. V. Budny, Nucl. Fusion **34**, 1247 (1994).
[7]H. Anderson *et al.*, Plasma Phys. Controlled Fusion **42**, 781 (2000).
[8]H. P. Summers, See http://www.adas.ac.uk/manual.php for "The ADAS User Manual v2.6".
[9]L. Dectyarev and V. Drozdov, Comput. Phys. Rep. **2**, 341 (1985).
[10]R. V. Budny, D. Coster, D. Stotler, M. G. Bell *et al.*, J. Nucl. Mater. **196–198**, 462 (1992).
[11]S. I. Krasheninnikov, L. E. Zakharov, G. V. Pereverzev, Phys. Plasmas **10**, 1678 (2003).